Mid-Complexity Circuital Model of Induction Motor with Rotor Cage: a Numerical Resolution

A. Marfoli, P. Bolognesi, L. Papini and C. Gerada, *Senior, IEEE*

***Abstract*—A general middle complexity model of electro-magnetic devices is applied to a cage induction motor. Such modelling approach has been simplified and adapted in order to pursue a fair representation of the electrical machine. Particular attention was given to the rotor cage, proposing a simplified representation exploiting the symmetry of the cage itself. A comparative analysis vs the results provided by a finite element model is also presented for validation purposes aiming to assess the accuracy of the proposed method.**

***Index Terms*—Inductances, Induction Motor, Numeric-analytical, Rotor cage, Slotting effects, Winding function**

I. Introduction

Even though Squirrel Cage Induction Motor (SCIM) have been extensively studied over the years, the design and analysis of such machine is currently attracting attention due to the increasing efficiency demand and stricter emission regulations. An accurate steady state and dynamic performance prediction of SCIM is a key tool for the design process, provided that it features fast computation and good accuracy. To fulfil the requirements of rated mechanical power and starting capabilities, Finite Element (FE) analysis in time domain is undoubtedly the most accurate tool to predict the motor performance. However, the high accuracy of the numerical approach comes at the cost of high computational effort due to the induced nature of the rotor currents. Alternatively, the steady state equivalent mono-phase circuit is a valid approach to predict the motor performance. For such model, the trade-off between accuracy and fast computation is in fact presented in [1]. Increased accuracy is achieved in [2] and [3] when the dependency of the lumped parameters with respect to the currents and rotor frequency is investigated by means of a set of dedicated FE simulations. However, such model cannot analyse the dynamic behaviour of the machine. In order to pursuit a circuital representation able to account the time dependency of the motor behaviour with respect to the state variables (currents and rotor position), a full circuital model based on the electro-magneto-mechanical equations is required. The general approach to model an electro-magnetic device is extensively explained in literature, [4] and [5]. Under appropriate assumption, the method applies the electro-magnetic field laws to the geometry of the main airgap of the device, considered the region in which the main part of the electro-magnetic energy is stored and the electro-mechanical energy conversion occurs. In [4], an accurate summary of the formulation that aims to describe the main phenomena for a general electro-magnetic device is presented. Moreover, in [5], additional constrains were included in the analysis in order to adapt such treatment for rotary electrical machines. Although the general framework of such analysis is well detailed in the metioned papers, further considerations and assumptions are needed when the SCIM is analysed. For instance, in [6], [7] a method of modelling SCIMs in transient conditions is developed. The stator and rotor slotting effects are neglected in both analyses. Increase accuracy can be achieved when accounting for the effects of the slot openings as presented in [8], [9]. In [8], the air gap thickness has been considered as a sum of two separate air gaps and approximated with a trapezoidal shape. In [9] the slotting effect is included in the permeance function as extensively reported in [10].

This paper deals with the implementation of a numeric-analytical method applied to SCIM based on a generalized approach to analyse electro-magnetic devices. The investigation performed aims to validate the flexibility and accuracy of the method. A simplified modelling of the slotting effects is proposed and particular attention is given to the rotor cage, proposing a compact representation by exploiting the symmetry of the cage itself as reported in [11] for synchronous generators. Similar approach is applied to the SCIM under investigation. The results provided by this method, such as inductances profiles against position and electro-magnetic torque in specific conditions are validated by means of a FE model purposely developed. Such comparison proves the effectiveness of the proposed method, as highlighted in Section IV.

II. Analytical model

The lumped parameters equivalent circuit is widely used to model electro-magnetic devices and electrical machines. However, achieving an effective representation of the slotting effects and the rotor cage is still a challenging task. Although the general framework of the modelling [5] was maintained in this work, further considerations and assumptions are made to pursue a better representation of the SCIM. Hereafter a detailed description of the considered model is reported, including the related simplifying hypothesis.

This work was supported by ABB Corporate Research

A. Marfoli, P. Bolognesi, L. Papini and C. Gerada are with the Power Electronics, Machines and Control (PEMC) Group, University of Nottingham, Nottingham, UK (e-mail: alessandro.marfoli@nottingham.ac.uk), (e-mail: p.bolognesi@ieee.org), (e-mail: luca.papini@nottingham.ac.uk), (e-mail: chris.gerada@nottingham.ac.uk)

- Coaxial and equal length of stator and rotor cores separated by a narrow airgap.
- Stator and rotor length larger than the external radius of the stator core.
- Closed shape and straight-parallel active sides of the windings.
- Negligible magneto motive force drop, hysteresis losses and eddy current in the stator and rotor yokes.
- Negligible influence of the secondary flux tubes over the geometrical displacement of the main flux tubes in the air gap.
- Absence of skin effects in the solid bars of the rotor.
- Minor radial variation of the magnetic field in the airgap.
- High relative permeability and linear behaviour of the iron core's material.

A. *Cage modelling*

The cage structure consists of a group of parallel paths connected by means of low resistance connections located in the end region. The whole set of connections composing the ring of the cage are important to be modelled as enables to account for the effect of the current distribution in the short circuit ring of the rotor cage. A complete cage featuring b bars can be than represented by means of an equivalent planar topology depicted in Fig. 1, where the inner and outer circles represent the two end rings.

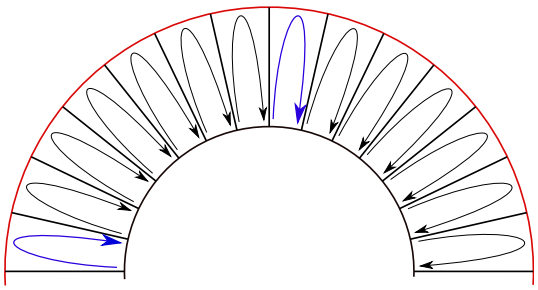

Fig. 1: Planar representation of the rotor cage with current loops

As illustrated in [11], each loop is delimited by adjacent bars and relative front connection and can be considered as an equivalent phase in short circuit condition. The voltage drop in each section of the loop needs to be taken into account, including the inner and outer connections of the planar representation. The current in each bar is then computed as the difference of the currents flowing in adjacent loops: this means that the resistance matrix R related to the cage assumes the following tridiagonal form:

$$R = \begin{bmatrix} R_s & R_m & 0 & \cdots & \cdots & 0 & R_m \\ R_m & R_s & R_m & 0 & \cdots & \cdots & 0 \\ 0 & R_m & R_s & R_m & 0 & \cdots & 0 \\ \vdots & \ddots & \ddots & \ddots & \ddots & \ddots & \vdots \\ 0 & \cdots & 0 & R_m & R_s & R_m & 0 \\ 0 & \cdots & \cdots & 0 & R_m & R_s & R_m \\ R_m & 0 & \cdots & \ldots & 0 & R_m & R_s \end{bmatrix} \quad (1)$$

where $R_s = 2 \cdot (R_{Bar} + R_{Ring})$ and $R_m = -R_{Bar}$ can be labelled as self-resistance and mutual resistance, respectively. According to the assumptions concerning the shape of cores and distribution of the windings, the axial component of the magnetic field results negligible and the electromagnetic problem can be approximate as bi-dimensional. However, the modelling of an electrical machine equipped with a cage structure requires further considerations. In fact, applying the Gauss law to the closed surface obtained by joining the elementary surfaces delimited by the adjacent bars and related end ring sections leads to the integral form of the divergence free equation for the magnetic flux density field $\hat{B}$ as expressed in eq. (2).

$$\nabla \cdot \hat{B} = 0 \rightarrow \int_{Main} \hat{B} \cdot \hat{n}\, dS + \int_{Caps} \hat{B} \cdot \hat{n}\, dS = 0 \quad (2)$$

In a 2D scenario, the flux linkage contribution due to the caps is neglected, so (2) can be written as (3); assuming linear behaviour of the soft ferromagnetic materials, equation (3) can be arranged as in (4).

$$\int_{Main} \hat{B} \cdot \hat{n} dS = \sum_k \psi_{rk} = \hat{1}^T \cdot \hat{\psi}_r = 0 \quad (3)$$

$$\bar{1}^T \cdot [L_{rs} \quad L_{rr}]_\alpha \cdot \begin{bmatrix} \bar{i}_s \\ \bar{i}_r \end{bmatrix} = 0 \quad \forall \quad (\bar{i}, \alpha) \quad (4)$$

where L_{rs} is the stator-rotor mutual inductances matrix and L_{rr} is the rotor self and mutual inductances matrix. $\bar{i}_s$ and $\bar{i}_r$ are the stator and rotor currents respectively and α is the Lagrangian variable describing the mechanical state of the device. Considering (4), can be concluded that the matrix of the inductances $L(\alpha)$ is singular. Therefore, a rotating machine featuring a squirrel cage cannot be treated completely as a 2D case, meaning that the end ring effects (resistance and leakage inductance) cannot be neglected.
The end ring effects were then computed analytically. As a first approximation, the leakage inductance was estimated using eq. (5) reported in [12].

$$L_{ring} = \mu_0 \cdot \frac{b}{m \cdot p^2} \cdot \frac{1}{3} \cdot \left[(l_{bar} - l_s) + \upsilon \cdot \frac{\pi \cdot D_r}{2p} \right] \quad (5)$$

where p is the number of pole pairs, b and m are the number of bars and stator phase respectively, l_{bar} is the length of the rotor bar, l_s is the length of the stator and D_r is the average diameter of the short-circuit ring. The factor υ is selected to be $\upsilon = 0.18$ for $p > 1$. The resistance was estimated considering a uniform distribution of the current density in the frontal connection between adjacent bars. Thus, the DC resistance was calculated as follows

$$R_{ring} = \rho_{Al} \cdot \frac{\pi D_{ring}}{b \cdot S} \quad (6)$$

where ρ_{Al} is the resistivity of aluminium, D_{ring} is the average diameter of the ring and S is the cross section of the ring.

B. General analytical equation

The generic analytical equations defining an electromagnetic device [5] are summarized hereafter. According with the hypotheses presented in Section II, the terminal voltage equation is expressed as follows

$$\bar{v}(t) = R \cdot \bar{i}(t) + \bar{M}(\alpha, \bar{i}) \cdot \frac{\partial \alpha(t)}{\partial t} + L(\alpha) \cdot \frac{\partial \bar{i}(t)}{\partial t} \quad (7)$$

where the vector $\bar{i}$ consists of the stator and rotor currents flowing in each equivalent phase, R is the matrix of resistances, $L(\alpha)$ the matrix of inductances which is represented as function of the sole variable α defined as the relative position between stator and rotor under the assumption of linear magnetic behaviour of ferromagnetic materials. The motional coefficient vector $\bar{M}(\alpha, \bar{i})$ is obtained as reported in eq. (8)

$$\bar{M}(\alpha, \bar{i}) = \left(\frac{\partial L(\alpha)}{\partial \alpha}\bigg|_{\hat{\alpha}} \right) \bar{i}(t) \quad (8)$$

The matrix of the inductances which account for the main fluxes defined as (i.e. those crossing the airgap) linked with the phases is expressed in the following:

$$L(\alpha) = \frac{l}{2\pi} \cdot \int_0^{2\pi} \mu_e(\gamma, \alpha) \cdot \bar{N}_E(\gamma, \alpha) \cdot \bar{N}_E(\gamma, \alpha)^T \cdot d\gamma \quad (9)$$

In eq.(9), l is the axial length of the motor, $\mu_e(\gamma, \alpha)$ is the equivalent permeability defined in eq. (10) as a function of the rotor position α and the tangential coordinate γ.

$$\mu_e(\gamma, \alpha) = \mu_0 \cdot \frac{\tau_g(\gamma, \alpha)}{\epsilon_g(\gamma, \alpha)} \quad (10)$$

In eq. (10), the function $\epsilon_g(\gamma, \alpha)$ represents the thickness of the air gap which account the distance between stator and rotor as well as the depth of the slot openings: it is expressed as the sum of partial thickness related to the rotor and stator as shown in eq. (11).

$$\epsilon_g(\gamma, \alpha) = \epsilon_s(\gamma, \alpha) + \epsilon_r(\gamma, \alpha) \quad (11)$$

The function $\tau_g(\gamma, \alpha)$ of eq. (10) define the profile of the medium magnetic-equipotential surface [5] in the air gap for every position α along the geometric tangential coordinate γ. Furthermore, $\bar{N}_E(\gamma, \alpha)$ is the vector of the equivalent winding functions of each phase of the machine as reported in eq. (12).

$$\bar{N}_{E(\gamma,\alpha)} = \bar{N}_{(\gamma,\alpha)} - \int_0^{2\pi} \frac{\mu_{e(\gamma,\alpha)}}{\int_0^{2\pi} \mu_{e(\gamma,\alpha)} \cdot d\gamma} \cdot \bar{N}_{(\gamma,\alpha)} \cdot d\gamma \quad (12)$$

Finally in (13), the expression of the torque is calculated from the derivative of the coenergy with respect to the position at fixed currents, which can be written as a product between current vector and the motional coefficient vector in the case of linear magnetic material's behaviour.

$$T(\alpha, \bar{i}) = \frac{\partial C_E(\alpha, \bar{i})}{\partial \alpha}\bigg|_{\bar{i}=\tilde{\bar{i}}} = \frac{1}{2} \cdot \tilde{\bar{i}}^T \cdot \bar{M}(\alpha, \tilde{\bar{i}}) \quad (13)$$

C. Case study

The analysis introduced in Section I, II-A and II-B is implemented to a medium size 3-phase SCIM with a rated power of 11 kW, 2 pole pairs, distributed single layer stator winding Y-connected and equipped with a set of 7 bars per pole on the rotor. The machine has been designed for applications at constant speed of 1500 [rpm]. In Fig. 2, the FE reference model developed for the analysis and the solution mesh are presented.

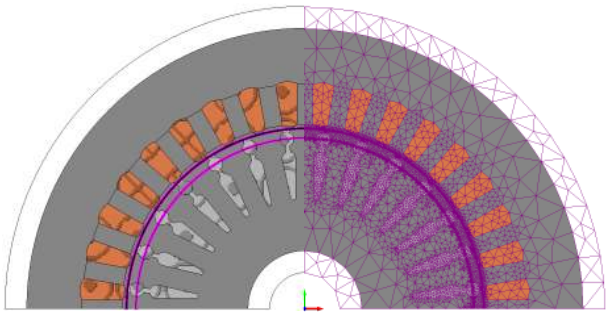

Fig. 2: FE model with a mesh representation

D. Slotting effects

The slotting effects of the machine under investigation can be accounted by means of slotting functions $\epsilon_s(\gamma, \alpha)$ and $\epsilon_r(\gamma, \alpha)$ of the stator and the rotor respectively. $\tau_g(\gamma, \alpha)$ is selected to achieve a fair representation of the medium magnetic equipotential surface in the airgap [5]. In Fig. 3, the functions $\epsilon_s(\gamma, \alpha)$ and $\epsilon_r(\gamma, \alpha)$ and their sum are represented respectively in black, red and blue lines, for a specific rotor position. Due to the small anisotropy introduced by the slot openings and having the air gap radius far greater than the slot openings depths, is reasonable to assume the medium magnetic-equipotential surface of the air gap as a perfect cylinder: $\tau_g(\gamma, \alpha) \approx 2 \cdot \pi \cdot r_g = const.$

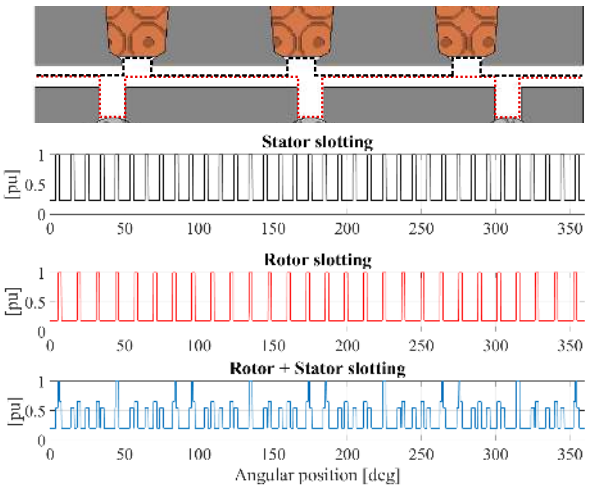

Fig. 3: Slotting functions vs angular position in pu: black line $\epsilon_s(\gamma, \alpha)$, red line $\epsilon_r(\gamma, \alpha)$ and blue line $\epsilon_s(\gamma, \alpha)$+$\epsilon_r(\gamma, \alpha)$

However, such simplification could lead to alteration of the inductances profile. In order to improve the accuracy, τ_g was

selected as the average between internal stator radius and external rotor radius as in eq. (14).

$$\tau_g(\gamma,\alpha) = 2\cdot\pi\cdot(r_g + (\epsilon_s(\gamma,\alpha) - \epsilon_r(\gamma,\alpha))/2) \qquad (14)$$

The top of Fig. 4 highlights in dot-red line the ideal profile of the medium magnetic-equipotential line in the air gap, while the black line is the approximated profile obtained implementing eq. (14). In Fig. 4 on the bottom, the function $\tau_g(\gamma,\alpha)$ calculated numerically is represented in pu as a function of γ at a specific α.

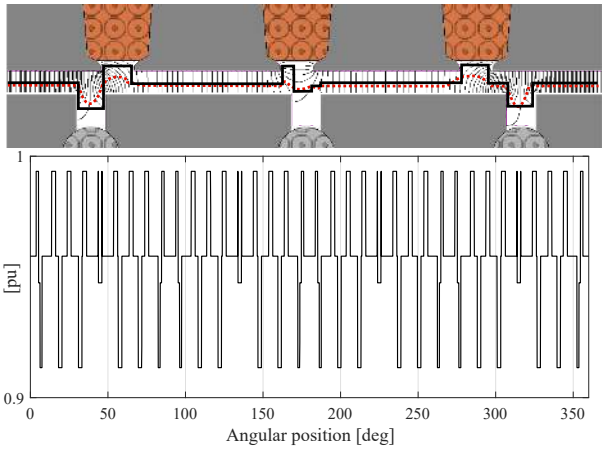

Fig. 4: Profile of the medium magnetic equipotential line in pu: $\tau_g(\gamma,\alpha)$

E. Modelling and representation of the rotor cage

In a cage structure featuring a set of bars having equal cross section, the current flowing in each bar exhibits, unless very unusual operating conditions, a sinusoidal distribution along the circumferential development of the rotor. Due to the symmetry property of such distribution, the current flowing in a loop under a pole is identical to the one of the loop placed at a pole pair pitch and it is opposite with respect to the loop located at a pole pitch distance. This considerations allow to model each equivalent rotor phase as series and anti-series connections of loops as shown in Fig. 5.

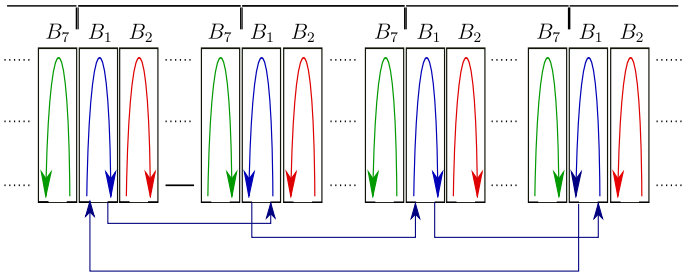

Fig. 5: Simplified representation of the current loops by exploiting the symmetry of the cage

The rotor cage can be therefore modelled with a set of $b/(2\cdot p)$ equivalent rotor phases. The rotor cage description presented enables to reduce the total number of equivalent phases from 3 (stator) + 28 (rotor) to 3 (stator) + 7 (rotor), thus reducing the model complexity and computational burden. However, the matrix of the resistances needs to be modified as in eq. (15) in order to take into account the new value of resistances of each equivalent rotor phase.

$$R = 4\cdot\begin{bmatrix} R_s & R_m & 0 & 0 & 0 & 0 & R'_m \\ R_m & R_s & R_m & 0 & 0 & 0 & 0 \\ 0 & R_m & R_s & R_m & 0 & 0 & 0 \\ 0 & 0 & R_m & R_s & R_m & 0 & 0 \\ 0 & 0 & 0 & R_m & R_s & R_m & 0 \\ 0 & 0 & 0 & 0 & R_m & R_s & R_m \\ R'_m & 0 & 0 & 0 & 0 & R_m & R_s \end{bmatrix} \qquad (15)$$

The mutual resistance between loop 1 and loop 7 is $R'_m = R_{Bar}$, in agreement with the relative current directions shown in Fig. 5.

III. Numerical resolution

The validation of the modelling method described in Section II is numerically implemented. The representation of the inductances matrix taking into account the geometric features of the SCIM under investigation is developed. In Section III-A the inductances against rotor position α computed numerically are compared with respect the FE results. The arrangement of such quantities in look-up tables, in particular the matrix $\partial L(\alpha)/\partial\alpha$ and $L(\alpha)^{-1}$, enables the numerical resolution of the model with the Matlab-Simulink platform. Further validation are presented to highlight the symmetrical behaviour of the rotor cage by means of comparing the full model with the simplified rotor cage model.

A. Inductances identification

The identification of $L(\alpha)$ is performed numerically off-line using eq. (12). The main inductances of such matrix are compared against a set of multi-static simulation, supplying alternatively the stator and rotor phases of a FE model aiming to identify the dependency of such quantities with respect to the rotor position. In Fig. 6 and Fig. 7 the self and mutual inductance respectively of a stator winding is shown as a function of the angular position α.

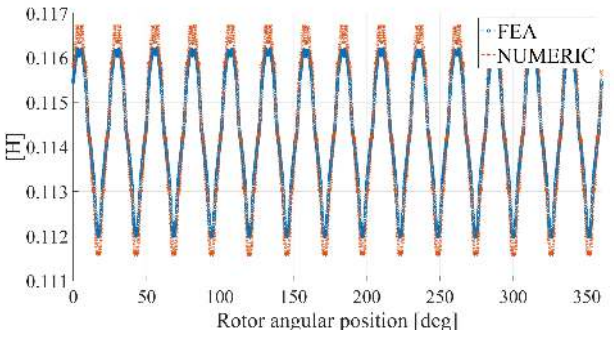

Fig. 6: $L_{s_i s_i}(\alpha)$: Stator self-inductance vs rotor angular position

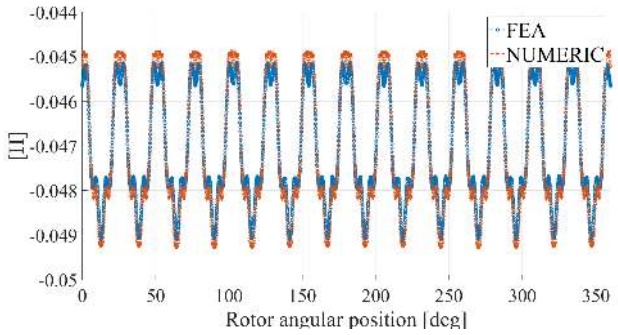

Fig. 7: $L_{s_j s_i}(\alpha)$: Stator mutual-inductance vs rotor angular position

In Fig. 8 and Fig. 9 the mutual inductance between a stator winding and a rotor winding is shown as a function of the rotor position. An overall good match of those profiles enables to assume a fair representation of the real distribution of the flux lines into the air gap.

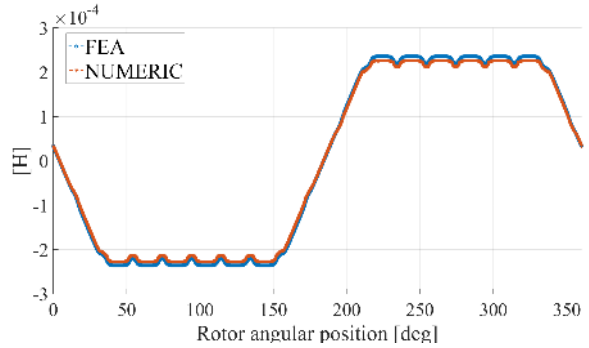

Fig. 8: $L_{s_j r_i}(\alpha)$: Stator-rotor mutual inductance vs rotor angular position

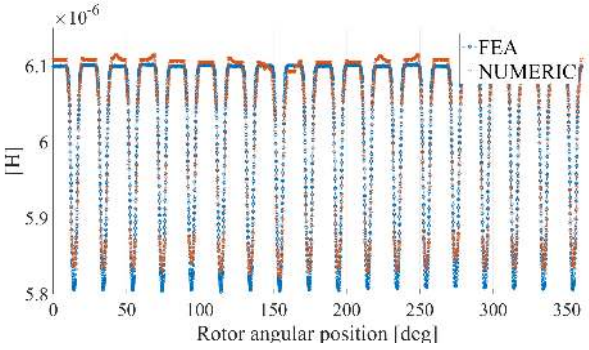

Fig. 9: $L_{r_j r_i}(\alpha)$: Rotor self inductance vs rotor angular position

B. Symulink model

A Matlab-Simulink model is built to calculate stator and rotor winding currents. As shown in Fig. 10, the input quantities of the model are the voltages imposed to the stator and rotor windings. The latter, due to the short circuit nature of their connections, exhibit a null value. The scheme displayed in Fig. 10 highlights in red line an additional connection which allows to simulate the real set up of the stator windings. In fact, as mentioned in Section II-C, the stator windings are Y-connected to a common node representative of the reference of the phase voltages.

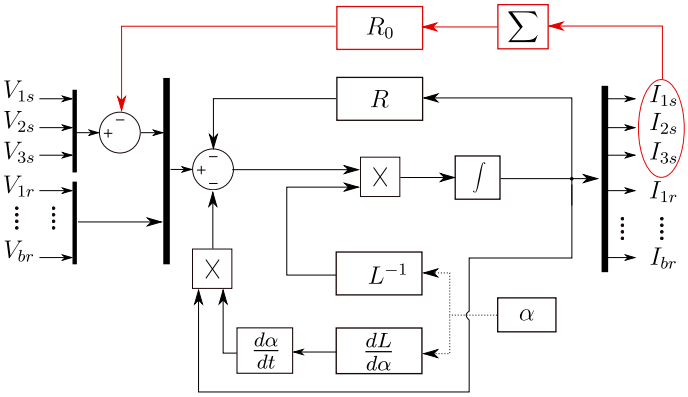

Fig. 10: Matlab-Simulink block diagram of the model

C. Simulation results

In this section the simulation results of the full rotor cage model are compared with the symmetric rotor cage model. The aim is to prove the symmetry property of the rotor winding constitute by loops placed at a pole pitch and a pole pair pitch distance and quantify the benefits relative to the simplified cage model in terms of computational time saving. The PC used for the analysis is a Intel Xeon with clock frequency of 3.5 GHz and 128 GB of RAM. A complete period of the rotor position is divided in 7560 divisions leading to an $L(\alpha)$ matrix featuring dimension of 31x31x7560 for the fully rotor cage while 10x10x7560 for the simplified cage structure. A group of rotor phases of the full rotor cage model with b = 28 are shown in Fig. 11.

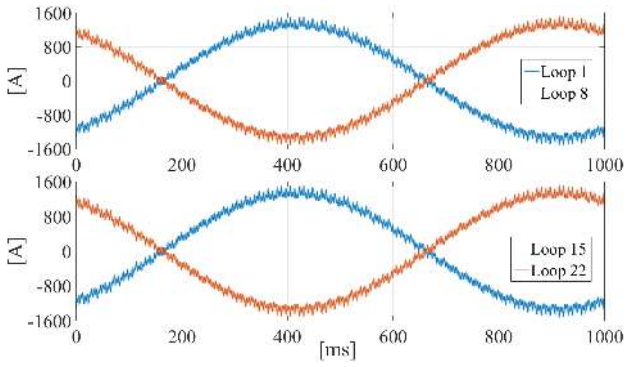

Fig. 11: Rotor loop current waveforms

The rotor phase windings constitute by loop currents 1-8 and 15-22 shown in Fig. 11 exhibit, as aspected, an anti-series trend. In fact, the currents flowing in the rotor loops placed at a pole pitch are equal and opposite. The current flowing in loops placed at a pole pair pitch, e.g. 1-15 and 8-22, exhibit the same profile. In Fig. 12 the currents of the rotor windings located at the same geometrical position are displayed for full

and symmetric cage model, respectively. A good match is exhibited between the two currents, confirming the reliability of the symmetric rotor cage model.

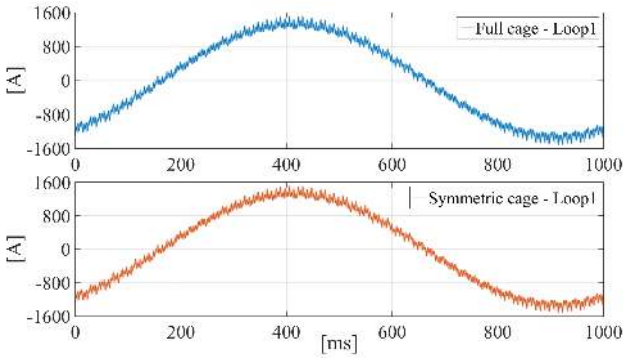

Fig. 12: Rotor loop current waveforms: Full vs symmetric cage

A comparison of the time consumed for the two models in term of off-line inductances computation, numerical resolution and data post-processing is presented in Table I. The simplified cage model allows to reduce the computational effort with respect to the full cage model without any impact over the accuracy of the currents computation.

TABLE I: Computational effort: full vs symmetric cage model

	Div	Off-line	Simulation	Post-proc.	Tot.
Full	7560	28'	25"	39"	29' 4"
Sym	7560	3'	3'	30"	6' 36"
Sym	25200	24'	3'	31"	27' 31"

IV. Results and FE validation

A further numerical resolution of the model has been performed considering a major number of divisions for each mechanical period in order to improve the accuracy of the outputs (circumferential coordinate discretized in 25200 elements). The symmetric rotor cage model permit a restrained impact over the computational effort as shown in Table I. The current of each stator and rotor winding is computed numerically while the current of each bar was computed in post-processing as the difference between adjacent loops. Finally, the torque profile was computed using eq. (13). The results are compared against a time step FE simulation supplying each stator phase with a set of balanced symmetrical voltages. The working points investigated are: no-load ($Slip = 0$), locked rotor ($Slip = 1$), load condition at $Slip = 0.5$ and nominal condition at $Slip = 0.02$. At no-load the currents induced in the rotor bars due to the first harmonic of flux density supported by the stator currents are null. However, the higher order harmonics of the flux density are asynchronous with respect to the rotor and therefore high order rotor currents are induced. In Fig. 13, Fig. 14, Fig. 15 and Fig. 16 a comparison of stator currents on the top and two rotor bars on the bottom are displayed, respectively. At lock-rotor condition Fig. 14, the stator and rotor currents exhibit a sinusoidal trend due to the constant permeance of the magnetic circuit.

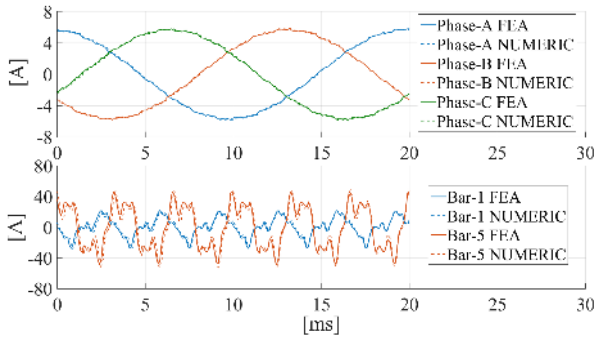

Fig. 13: Stator and rotor current waveforms: Slip = 0 [pu]

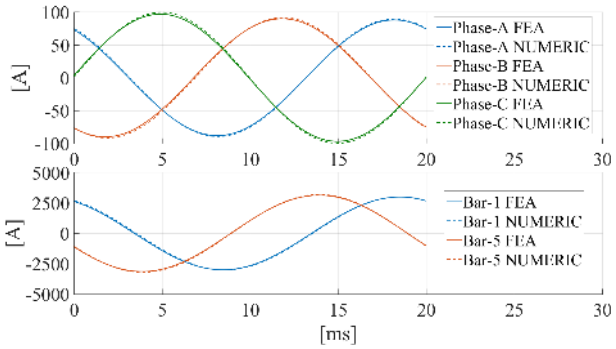

Fig. 14: Stator and rotor current waveforms: Slip = 1 [pu]

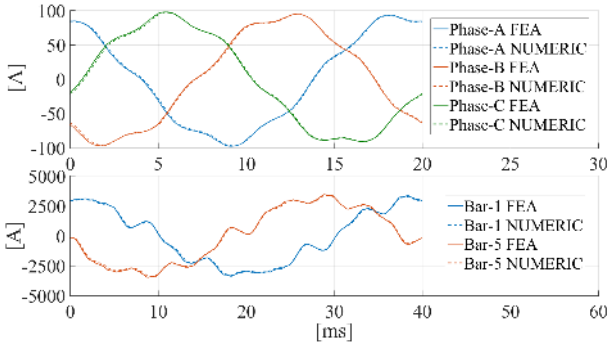

Fig. 15: Stator and rotor current waveforms: Slip = 0.5 [pu]

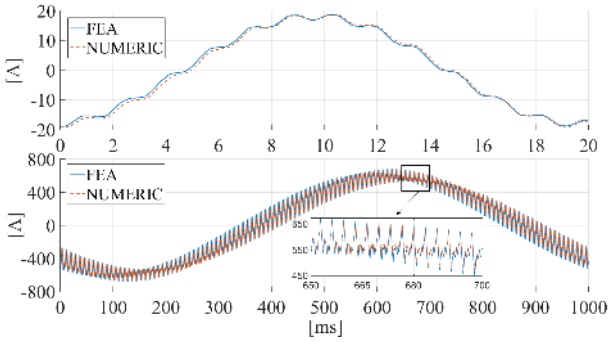

Fig. 16: Stator and rotor current waveforms: Slip = 0.02 [pu]

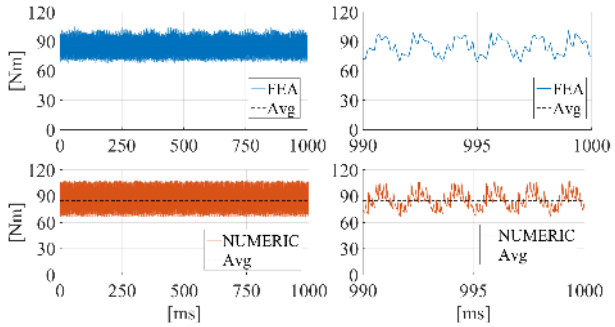

Fig. 17: Electro-magnetic torque waveforms: Slip = 0.02 [pu]

An overall good match is exhibited for all the operating conditions investigated. The SCIM produce the nominal mechanical power at rated slip of $0.02\,[pu]$. At this specific operating rotor frequency, the main output in term of currents and torque are shown in Fig. 16 and Fig. 17. In Fig. 17, the torque profile with respect to the time is displayed, considering a rotor electrical period on the left side of the graph and half of the last simulated stator period on the right side. A good match, exhibited also in term of torque profile Fig. 17, confirms the reliability of the circuital model of the SCIM under the assumptions reported in Section II. The adoption of a symmetric rotor model permit to increase the number of steps of a single rotor revolution, allowing an improved performance prediction.

V. Conclusion

This paper deals with an accurate estimation of the main quantities such as inductances, currents and torque profiles of a SCIM. A numeric resolution of a mid-complexity circuital model is implemented for a SCIM and particular focus was given to the rotor cage representation. Two different models are compared in order to prove the validity of the assumptions considered with the symmetric cage model. Advantages in term of computational time are highlighted and a comparison with an equivalent FE model is presented. The validity of the proposed methodology of modelling a SCIM, under simplified hypotheses, was proved. Such model will allow to investigate and analyse different motor topologies. Further work is on going aiming to include in the modelling the skin effects of the rotor bars, skewed cage and rotor layout with closed rotor bars.

References

[1] L. Alberti, N. Bianchi, and S. Bolognani, "A very rapid prediction of im performance combining analytical and finite-element analysis," *IEEE Transactions on Industry Applications*, vol. 44, no. 5, pp. 1505–1512, Sept 2008.

[2] A. Marfoli, L. Papini, P. Bolognesi, D. Genovese, and C. Gerada, "Analysis of induction machine: Comparison of modelling techniques," in *2017 IEEE International Electric Machines and Drives Conference (IEMDC)*, May 2017, pp. 1–7.

[3] D. Genovese, P. Bolognesi, M. D. Martin, and F. Luise, "A contextual parameter identification method for the equivalent circuit of induction machine," in *2016 XXII International Conference on Electrical Machines (ICEM)*, Sept 2016, pp. 25–31.

[4] P. Bolognesi, "Generalized circuital modeling of electromagnetic devices," *Proc. of ICEM 2004 Conf., Cracow, Sep. 2004.*, 2004.

[5] P. Bolognesi, "A mid-complexity analysis of long-drum-type electric machines suitable for circuital modeling," in *2008 18th International Conference on Electrical Machines*, Sept 2008, pp. 1–5.

[6] H. A. Toliyat and T. A. Lipo, "Transient analysis of cage induction machines under stator, rotor bar and end ring faults," *IEEE Transactions on Energy Conversion*, vol. 10, no. 2, pp. 241–247, Jun 1995.

[7] G. Joksimovi, "Parameterized dynamic model of cage induction machine," in *2016 XXII International Conference on Electrical Machines (ICEM)*, Sept 2016, pp. 513–518.

[8] G. Joksimovi, J. Riger, T. Wolbank, N. Peri, M. Vaak, G. Stoji, and V. Lei, "Dynamic induction machine model accounting for stator and rotor slotting," in *2012 XXth International Conference on Electrical Machines*, Sept 2012, pp. 207–212.

[9] S. Nandi, "Modeling of induction machines including stator and rotor slot effects," *IEEE Transactions on Industry Applications*, vol. 40, no. 4, pp. 1058–1065, July 2004.

[10] B. Heller and V.Hamata, *Harmonic field effects in Induction Machine*, N. Y. Elsevier, Ed., 1977.

[11] S. Nuzzo, P. Bolognesi, M. Galea, and C. Gerada, "A hybrid analytical-numerical approach for the analysis of salient-pole synchronous generators with a symmetrical damper cage," in *2017 IEEE International Electric Machines and Drives Conference (IEMDC)*, May 2017, pp. 1–8.

[12] T. J. Juha Pyrhonen and V. Hrabovcov, *Design of Rotating Electrical Machines*. John Wiley & Sons, Ltd, 20008.

VI. Biographies

Alessandro Marfoli Received the M.Sc. in electrical engineer from the University of Pisa, Pisa, Italy in 2015. He is actually working toward the PhD degree in electrical and electronic engineer at the Power Electronics, Machines and Control group, University of Nottingham, Nottingham, UK. His main research interest is analytical modelling and optimization for Induction Motor.

Paolo Bolognesi Received his M.Sc. and Ph.D. degrees in Electrical Engineering from the University of Pisa in 1995 and 1999, respectively. He joined then the University of Pisa as a post-doc junior researcher and finally as a Senior Researcher and Appointed Professor since 2001. His research interests span from modeling, analysis and design of electromagnetic devices, including unconventional electric machines and electromechanical actuators, to innovative topologies and modulation methods for static converters, also for applications related to electric and hybrid vehicles.

Luca Papini received the B.Sc. (Hons.) and the M.Sc. (Hons.) in electrical engineering from the University of Pisa, Pisa, Italy, in 2009 and 2011, respectively. From June to November 2011, he collaborated with the Department of Energy Engineering, University of Pisa, as a Research Assistant. In 2016 received the Ph.D. in electrical engineering form the University of Nottingham, Nottingham, U.K. Since 2013, he has been a Research Assistant with the University of Nottingham. His main research interests include high-speed, high power density electric machines, control, and levitating systems.

Chris Gerada (SM14) received the Ph.D. degree in numerical modelling of electrical machines from the University of Nottingham, Nottingham, U.K., in 2005. Since 2006, he has been the Project Manager of the GE Aviation Strategic Partnership. In 2008, he was appointed as a Lecturer in electrical machines; in 2011, as an Associate Professor; and in 2013, as a Professor at the University of Nottingham. His research interests include the design and modeling of high-performance electric drives. Prof. Gerada serves as an Associate Editor for the IEEE TRANSACTIONS ON INDUSTRY APPLICATIONS and as the Chair of the Electrical Machines Committee of the IEEE Industrial Electronics Society